Available online at www.sciencedirect.com
SCIENCE DIRECT®
International Journal of Heat and Mass Transfer 48 (2005) 5520–5535
International Journal of HEAT and MASS TRANSFER
www.elsevier.com/locate/ijhmt

Thermal convection for a thermo-dependent yield stress fluid in an axisymmetric horizontal duct

C. Nouar

LEMTA, UMR 7563 (CNRS—INPL—UHP), INPL, ENSEM, 2 avenue de la Forêt de Haye, BP 160, 54504 Vandœuvre-lès-Nancy Cedex, France

Received 2 March 2004; received in revised form 29 March 2005
Available online 24 August 2005

Abstract

This paper deals with the combined forced and free convection heat transfer of a yield stress fluid in a horizontal duct heated uniformly with a constant heat flux density. It is assumed that (i) the rheological behavior of the fluid can be described by the Herschel–Bulkley model and that the consistency K^* varies with temperature T^*, as $K^* = a\exp(-bT^*)$; (ii) the variation of the fluid density ρ, with temperature, $\rho = \rho_e(1 - \beta(T^* - T_e^*))$, is considered important only in the buoyancy term and (iii) the Péclet number is sufficiently large so that it is possible to resort to an asymptotic solution. The aim of this study is to quantify the effect of the rheological properties on the magnitude of the secondary flows induced by the thermo-dependency of K^* and ρ. Expressions for local Nusselt number and wall shear stress are given. Finally, to be consistent with the variation along the duct of the axial velocity in the central zone around the axis, due to the thermo-dependency of K^* or ρ, the pseudo-plug zone and pseudo-yield surface notions are introduced. Some characteristics of the stresses distribution within the pseudo-plug zone are discussed.

Keywords: Forced convection; Free convection; Yield stress fluid; Thermo-dependent consistency

1. Introduction

Heat transfer in non-Newtonian fluids is of practical importance in many industrial applications for example in paper making, drilling of petroleum products, slurry transportation and processing of food and polymer solutions. The literature reviews made by Cho and Hartnett [1] and Shenoy and Mashelkar [2] show that the thermal convection in yield stress fluids has received little attention prior to 1982, despite the fact that they are frequently encountered in the above-mentioned engineering processes. Bird et al. [3] gave a list of materials that fall into this category of fluids. In the two last decades, very few papers dealing with the thermal convection for a yield stress fluids were published. In the following section, the heat transfer characteristics of such fluids in laminar flow in plane channel, circular duct or annular duct described in the literature are summarized.

1.1. Literature review

Forced convection in Bingham fluids in a circular pipe with uniform wall temperature, assuming fully developed flow and thermally developing field (Graetz

E-mail address: cherif.nouar@ensem.inpl-nancy.fr

0017-9310/$ - see front matter © 2005 Elsevier Ltd. All rights reserved.
doi:10.1016/j.ijheatmasstransfer.2005.06.016

problem), was considered by Hirai [4] and Wissler and Schechter [5]. Under additional assumptions of constant rheological properties and negligible both axial conduction and viscous dissipation, the energy equation was solved by separation of variables method leading to an eigenvalue problem. They determined numerically the first seven eigenvalues and eigenfunctions for different yield stress (τ_y) to wall shear stress (τ_w) ratios $r_0 = \tau_y/|\tau_w| = 0$, 0.25, 0.5, 0.75 and 1. Later, Blackwell [6] found that the number of eigenvalues was not sufficient to evaluate the heat transfer coefficient, particularly near the entrance section of the heating zone. Then, he extended the calculations to include the first 60 eigenvalues. The axial variation of the Nusselt number, Nu, was computed for $r_0 = 0$, 0.2, 0.4, 0.6, 0.8 and 1.0. As expected, Nu increases with increasing r_0, because of the increase of the wall velocity gradient. Johnston [7] solved the Graetz problem by including the axial conduction term in the energy equation. He concluded that, in order to ignore the axial conduction the Péclet number, Pe (defined with the bulk velocity and the diameter of the pipe), must be greater than 1000. Min et al. [8] extended the Graetz problem by taking into account both axial conduction and viscous dissipation. The authors showed that the heat transfer characteristics in the entrance region were significantly affected by the yield stress when including the viscous dissipation. This effect was also observed in the case of uniform wall heat flux [9]. The simultaneous development of the hydrodynamic and thermal fields in the entrance region of circular pipe for Bingham fluid was first considered by Vradis et al. [10]. Uniform wall temperature and constant rheological properties were assumed. The fully elliptic governing equations including the viscous dissipation term were solved numerically. The results were presented for Prandtl, Pr, and Brinckman, Br, numbers in the range of $[0.1, 1]$ and for Reynolds number of order 10. As expected, the larger the yield stress the shorter is the dynamic entrance length. In addition, as for the situation of thermally developing flow, the numerical results indicated that the yield stress effect became more significant when the viscous dissipation was taken into account. Min et al. [11] revisited the problem considered by Vradis et al. [10] and gave more accurate numerical results. However, same trends were observed for the yield stress effects.

In the previous studies, the fluid rheological properties were considered independent of temperature. This can be a serious assumption since, in many cases this effect has a significant influence on heat transfer coefficient. Forrest and Wilkinson [12] analyzed the heat transfer for Herschel–Bulkley fluid flows inside tubes. It was assumed that the flow was fully developed at the entrance to the heated section. The axial conduction and the viscous dissipation as well as the radial velocity and the axial velocity gradients were neglected. The thermo-dependency of the rheological parameters is restricted only to the consistency as it is more significant. According to the authors, the yield stress is mainly dependent on a mechanical locking of the fluid which is essentially temperature independent. The resulting momentum and energy equations were solved numerically and the results were illustrated graphically. It was shown that a decrease of the consistency near the heated wall induced an increase of the wall velocity gradient and therefore that of the heat transfer coefficient. The range of the parameters considered by the authors was limited and it is difficult to interpolate their results for a general engineering design purposes. Naïmi et al. [13] studied experimentally the heat transfer for an aqueous solution of Carbopol 940 flow in an annular duct with a rotating inner cylinder. The outer cylinder was heated at constant heat flux density and the inner one was assumed adiabatic. The rheological behavior of the used fluid was described by a Herschel–Bulkley model with temperature-dependent consistency. They determined the evolution of the local Nusselt number and observed that: (i) the Nusselt number rose with the increasing imposed heat flux; (ii) this rise was more important when the inner cylinder was rotating with an angular velocity, Ω, such that the dimension of the plug zone was reduced to zero. Finally, the experimental results were presented in the form of Nusselt number correlation. The effect of the variation of the consistency, K^*, with temperature on heat transfer was described by a dimensionless number $\frac{b\Phi^* D_h}{2\lambda}$: $Nu \propto \left(\frac{b\Phi^* D_h}{2\lambda}\right)^t$, where b is the temperature exponent of K^*: $K^* = a\exp(-bT^*)$. The exponent, t, was set to 0.1 for Poiseuille flow and to 0.16 when the inner cylinder was rotating with a velocity such that the plug region was suppressed. According to these authors, the plug region inhibited the development of radial velocity and therefore limited the axial velocity deformation. Consequently, the thermo-dependent consistency effect was reduced. This tendency was also observed experimentally by Nouar et al. [14]. Indeed, using the same fluid as Naïmi et al. [13], Nouar et al. [14] analyzed the thermal convection for Herschel–Bulkley fluids in a circular duct with a constant heat flux density at the wall. The authors observed that for a given flow rate, when the concentration of Carbopol increases, the yield stress increases and the effect of the thermo-dependency of the consistency becomes less pronounced. Once again, correlations for the Nusselt number of the form $Nu \propto \left(\frac{b\Phi^* R^*}{\lambda}\right)^t$ were proposed, where the exponent t was determined as 0.1, 0.13 and 0.16 for 0.3, 0.2 and 0.1 w% Carbopol, respectively. Later, Nouar et al. [15], using the same experimental setup as that of Naïmi et al. [13], determined the critical angular velocity Ω_c, for which there was no central plug zone in the annular space. Then, the authors showed that the increase of the exponent, t, described in [13] was due in fact to the significant decrease of the wall velocity gradient at the heated wall when $\Omega > \Omega_c$. Soares

et al. [16] considered the situation of simultaneous development of dynamic and thermal fields in a duct with uniform wall temperature or uniform wall heat flux. The conservation equations including axial conduction were solved numerically and the results were presented graphically. It was demonstrated that neglecting the temperature dependence of material properties may introduce important errors in the heat transfer coefficient.

Very few authors introduced the effect of free convection on the heat transfer coefficient. Patel and Ingham [17,18] considered the case of fully developed mixed convection of Bingham fluid in a vertical parallel plate duct and in an eccentric annulus. Different flow configurations were determined according to the ratio of the Grashof number to the Reynolds. These results are probably more useful for the heat transfer processes in the flow of mud and cements in long oil wells during drilling and cementing. To our best knowledge, the problem of mixed convection for yield stress fluid in the thermal entrance region of a duct, heated with uniform heat flux, was not studied.

1.2. Motivation of the present study and its position with respect to the literature

For certain situations like the thermal treatment process in food industry, the determination of the heat transfer characteristics in the thermal entrance region is relevant to control the quality of the products. Indeed, for several food fluids (milk chocolate, dairy desserts, apple sauce, orange juice concentrate,...) concerned by this process, the associated Péclet number is very large ($Pe > 1000$), and therefore the thermal entrance length x_t^* is very large. For example, in the case of a duct, a simple scaling analysis shows that x_t^* is of order $Pe \times$ radius.

Actually, for thermo-sensitive products which cannot bear an abrupt variation of temperature, an electrical tube exchanger (from Actini) is used. It consists on series of tubes (made of stainless steel) heated by a direct passing an electrical current through the wall, so that a uniform heat flux density is imposed. The technical details of this kind of heat exchanger can be found in Ref. [19]. The diameter of the tube varies between 3×10^{-2} and 4×10^{-2} m and the mean velocity of the product is about 0.1 m/s. The Péclet number calculated using the specific heat and thermal conductivity of water is about 10^4, and x_t^* is approximately 150 m. One has also to note that for several food fluids, the thermo-dependency of the effective viscosity can be significant.

In the preceding literature review [13–15], this effect is taken into account through an empirical correction factor in the Nusselt correlations. There is no quantitative analysis of the velocity and temperature distribution. In addition, the effect of free convection is not clarified.

The present paper deals with the combined forced and free convection heat transfer of a thermo-dependent yield stress fluid in the thermal entrance region of a horizontal circular duct. It is assumed that the rheological behavior of the fluid can be described by the Herschel–Bulkley model. For unidirectional shear flow with velocity $u^*(y^*)$ in the x^* direction, the relationship between the shear stress τ_{xy}^* and the velocity gradient $\mathrm{d}u^*/\mathrm{d}y^*$ is:

$$\tau_{xy}^* = \mathrm{sgn}(\mathrm{d}u^*/\mathrm{d}y^*)\tau_y^* + K^* \left|\frac{\mathrm{d}u^*}{\mathrm{d}y^*}\right|^{n-1} \frac{\mathrm{d}u^*}{\mathrm{d}y^*} \Longleftrightarrow |\tau_{xy}^*| \geqslant \tau_y^*, \tag{1}$$

$$\mathrm{d}u^*/\mathrm{d}y^* = 0 \Longleftrightarrow |\tau_{xy}^*| < \tau_y^*, \tag{2}$$

where τ_y^* is the yield stress, n is the flow behavior index and K^* is the consistency. This yield stress fluid model is chosen because the results obtained here can also be used for Newtonian fluid ($n = 1, \tau_y^* = 0$), Ostwald De Waele fluid ($\tau_y^* = 0$) and Bingham fluid ($n = 1$), covering by this way a wide range of inelastic viscous fluids. The motivations of this work are (i) to understand and to quantify the effect of n and τ_y^* on the temperature and velocity distributions. We are particularly interested in their effect on the intensity of the secondary flows generated on one hand by the buoyancy forces and on the other hand by the thermo-dependency of the consistency; (ii) to provide expressions for the heat transfer coefficient and the wall shear stress; (iii) to give some characteristics on the stresses within the pseudo-plug.

The plan of the paper is as follows: The fundamental mechanisms which control the thermal convection for laminar flow of a yield stress fluid in a duct heated at a constant heat flux density are described in Section 2. The governing equations of the problem are given in Section 3. The methodology used for solving the problem is presented in Section 4. Here, an asymptotic analysis is adopted since the Péclet number, Pe, encountered for the fluids considered in the present study is very large ($Pe \geqslant 1000$). In addition this method leads to analytical expressions for the velocity components as well as for the heat transfer coefficient and the wall shear stress. The results are given and analyzed in Section 5. The validity domain of the asymptotic solution is determined in Section 6. Finally, a conclusion is given in Section 7.

2. Problem description

A laminar flow of an Herschel–Bulkley fluid in a circular duct of radius R^* is considered. For fully developed Poiseuille flow and isothermal conditions, the flow field comprises a plug core moving as a rigid body, with viscoplastic shear region adjacent to the wall. The

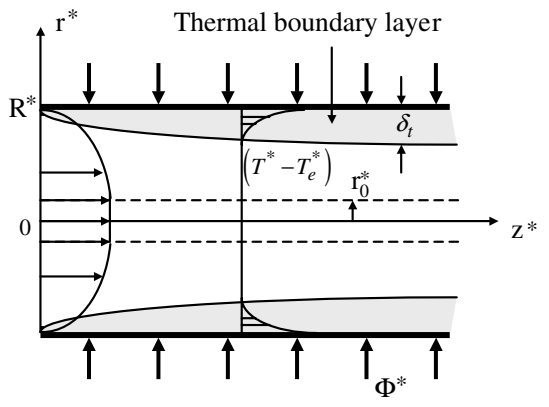

Fig. 1. Coordinate system and thermal boundary layer development along the heating zone. The dashed lines at r_0^* represent the yield surface position in isothermal situation.

ratio of the radius r_0^* of the plug zone to R^* depends only on the flow behavior index, n, and the Herschel–Bulkley number, Hb: ratio of a yield stress to a nominal viscous stress.

When the pipe wall is heated (here, at a constant heat flux density, Φ^*), a thermal boundary layer develops along the heating zone, starting from the inlet section as it is shown in Fig. 1. A temperature profile is also drawn to indicate that the temperature variations are confined mainly in the thermal boundary layer.

Due to the decrease of the consistency with temperature, T^*, the fluid is accelerated near the heated wall and decelerated in the central part of the duct for flow rate conservation. This motion causes fluid particles to move towards the heated wall (Fig. 2(a)). Simultaneously, due to the temperature difference between the wall and the inlet fluid, an upward flow is induced inside the thermal boundary layer by the buoyancy forces (Fig. 2(b)). The displacement of the secondary boundary layer induces a downward stream outside the thermal boundary layer. It results in a radial motion of fluid particles from the heated wall to the core flow in the upper half of the duct, $\pi/2 < \phi < \pi$, and from the core flow to the heated wall in the lower half of the duct, $0 < \phi < \pi/2$. Near the entrance section, the forced convection is the dominant mechanism. The effect of $K^*(T^*)$ is important close to the inlet section, then decreases along the heating zone. On the other hand, the buoyancy force effect increases along the heating zone. From a dimensionless axial position denoted by X_c^+, the buoyancy force effect becomes dominant. The present study is restricted to the domain, $X^+ < X_c^+$, where the forced convection is the convection dominant mechanism. As indicated in the introduction, one of the motivations of the present work is to determine the effect of the rheological parameters on the intensity of the secondary flows described above.

3. Governing equations

The fluid is assumed incompressible and the temperature dependence of τ_y^* and n are weak compared to the temperature dependence of K^* and thus can be ignored. The relation $K^* = a\exp(-bT^*)$ is adopted. At the entrance of the heated region, $z^* = 0$, the flow is fully developed and the fluid temperature T_e^* is constant and uniform. The radius of the plug zone is denoted by r_0^*. In this study, it is assumed that (i) the Péclet number, Pe, is sufficiently large ($Pe > 1000$), in order to neglect the axial diffusion [7], (ii) the viscous dissipation is very small and can be neglected and (iii) the variation of the fluid density with T^* : $\rho = \rho_e[1 - \beta(T^* - T_e^*)]$ is considered important only in the buoyancy force (Boussinesq approximation). Here, β is the coefficient of thermal expansion and $\rho_e = \rho(T_e^*)$ is the density of the fluid at the entrance temperature.

The dimensionless governing equations are:

$$\nabla \cdot \boldsymbol{V} = 0, \tag{3}$$

$$[\boldsymbol{V}_{,t} + (\boldsymbol{V} \cdot \nabla)\boldsymbol{V}] = -\nabla P + \frac{Gr}{Re^2}\theta\delta\boldsymbol{\xi} + \nabla \cdot \boldsymbol{\tau}, \tag{4}$$

$$\theta_{,t} + (\boldsymbol{V} \cdot \nabla)\theta = \frac{1}{Pe}\Delta\theta. \tag{5}$$

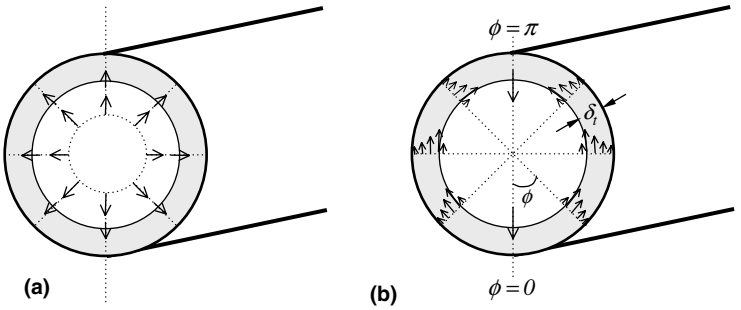

Fig. 2. (a) Secondary flow due to the thermo-dependency of K^*. The arrows represent the radial motion of the fluid particles to the heated wall. (b) Upward flow in the thermal boundary layer due to buoyancy forces.

Here P is the pressure, $\boldsymbol{V}$ is the velocity and $\boldsymbol{\tau}$ the deviatoric extra-stress tensor. The velocity vector is of the form $\boldsymbol{V} = u\boldsymbol{e}_z + v\boldsymbol{e}_r + w\boldsymbol{e}_\phi$, where u, v, w are the velocity components and $\boldsymbol{e}_z$, $\boldsymbol{e}_r$ and $\boldsymbol{e}_\phi$ are unit vectors in the axial z, radial r, and orthoradial ϕ directions, respectively.

$$\Delta = \left[\frac{\partial^2}{\partial r^2} + \frac{1}{r}\frac{\partial}{\partial r} + \frac{1}{r^2}\frac{\partial^2}{\partial \phi^2}\right] \quad \text{and} \quad \boldsymbol{\xi} = -\frac{\mathbf{g}}{g}.$$

In Eqs. (3)–(5), Gr, Re and Pe are the generalized Grashof, Reynolds and the Péclet numbers, respectively. They are defined by:

$$Re = \frac{\rho U_d^{*2-n} R^{*n}}{K_e^*}, \quad Gr = \frac{\rho_e^2 g\beta(\Phi^* R^*/\lambda)R^{*3}}{K_e^{*2}(U_d^*/R^*)^{2(n-1)}},$$
$$Pe = \frac{\rho C_p U_d^* R^*}{\lambda},$$

where C_p is the specific heat. The governing equations are rendered dimensionless by using the following scales:

$$z = \frac{z^*}{R^*}; \quad r = \frac{r^*}{R^*}; \quad u = \frac{u^*}{U_d^*}; \quad v = \frac{v^*}{U_d^*}; \quad w = \frac{w^*}{U_d^*},$$
$$\theta = \frac{(T^* - T_e^*)\lambda}{\Phi^* R^* \delta}; \quad P = \frac{P^*}{\rho_e U_d^{*2}}; \quad \tau_{ij} = \frac{\tau_{ij}^*}{\rho_e U_d^{*2}}; \quad K = \frac{K^*}{K_e^*},$$

where U_d^* is the bulk velocity, λ is the thermal conductivity, K_e^* is the fluid consistency evaluated at the entrance temperature and δR^* is characteristic scale of the thermal boundary layer. Writing a balance between the axial convection and normal conduction terms of the energy equation, we obtain $\delta = Pe^{-1/3}$.

Using the Von-Mises criterion, the scaled constitutive laws for the fluid are

$$\boldsymbol{\tau} = \frac{2}{Re}\mu_a \mathbf{D} \Longleftrightarrow (\tau_{II})^{1/2} > \frac{Hb}{Re}, \tag{6}$$

$$\mathbf{D} = 0 \Longleftrightarrow (\tau_{II})^{1/2} \leqslant \frac{Hb}{Re}, \tag{7}$$

with

$$\mu_a = \frac{Hb}{(4D_{II})^{1/2}} + \exp(-P_n\delta\theta)(4D_{II})^{(n-1)/2}, \tag{8}$$

where the Pearson number, Pn, the Herschel–Bulkley number, Hb, and the second invariants D_{II} and τ_{II} of the deformation rate and deviatoric stress tensors are defined by:

$$Pn = \frac{b\Phi^* R^*}{\lambda}; \quad Hb = \frac{\tau_y^* R^{*n}}{K_e^* U_d^{*n}}; \quad D_{II} = \frac{1}{2}(D_{ij}D_{ij});$$
$$\tau_{II} = \frac{1}{2}(\tau_{ij}\tau_{ij}),$$

where $D_{ij} = (1/2)(u_{i,j} + u_{j,i})$. The dimensionless number, Pn, traduces the thermo-dependency of the effective viscosity. Far from the entrance section, Pn represents the relative variation of the consistency between the wall and the axis. Concerning the boundary conditions: (i) At the entrance section, $z = 0$, the flow is fully developed with a uniform temperature, $\theta = 0$; (ii) on the wall a non-slip condition is considered and a constant heat flux density is applied; (iii) at the yield surface (surface where $(\tau_{II}^*)^{1/2} = \tau_y^*$), the velocity and stress are continuous.

For one-dimensional shear flow, the axial velocity profile is given by [3,14]:

$$u = \begin{cases} \dfrac{n}{n+1}\left(\dfrac{Hb}{r_0}\right)^{\frac{1}{n}}(1-r_0)^{\frac{n+1}{n}}; & 0 \leqslant r \leqslant r_0, \\ \dfrac{n}{n+1}\left(\dfrac{Hb}{r_0}\right)^{\frac{1}{n}}\left[(1-r_0)^{\frac{n+1}{n}} - (r-r_0)^{\frac{n+1}{n}}\right]; & r_0 \leqslant r \leqslant 1. \end{cases} \tag{9}$$

The dimensionless axial velocity gradient at the wall ($r = 1$), denoted by $\varphi = (\mathrm{d}u/\mathrm{d}r)_{r=1}$, has an important role in the analysis of the heat transfer results. It is given by:

$$\varphi = \left[\frac{Hb(1-r_0)}{r_0}\right]^{1/n}. \tag{10}$$

It can also be written as $\varphi = \Pi\varphi_{new}$, where φ_{new} is the dimensionless axial velocity gradient at $r = 1$ for Newtonian fluid ($\varphi_{new} = 4$ for a circular duct). Hence, Π represents the modification of the wall shear rate by the rheological behavior of the fluid in isothermal situation.

Since the bulk velocity is used to scale the flow, it follows that:

$$2\int_0^1 r\, u(r)\,\mathrm{d}r = 1. \tag{11}$$

Using Eq. (9), it can be shown after some algebra that r_0 satisfies the following relation:

$$0 = (1-r_0)^{3+m} - (3+m)(1-r_0)^{2+m} + \frac{(2+m)(3+m)}{2}(1-r_0)^{1+m} - \frac{(3+m)(2+m)(1+m)}{2}\left(\frac{r_0}{Hb}\right)^m, \tag{12}$$

where $m = 1/n$. For low and large Hb, the following asymptotic expressions are derived:

As $Hb \to 0$

$$r_0 = \left(\frac{n}{3n+1}\right)^n Hb - \frac{n}{2n+1}\left(\frac{n}{3n+1}\right)^{2n-1} Hb^2 + \mathrm{O}(Hb^3). \tag{13}$$

As $Hb \to \infty$

$$r_0 = 1 - C_1\left(\frac{1}{Hb}\right)^{\frac{1}{1+n}} - C_2\left(\frac{1}{Hb}\right)^{\frac{2}{1+n}} + \mathrm{O}\left(\left(\frac{1}{Hb}\right)^{\frac{3}{1+n}}\right), \tag{14}$$

with

$$C_1 = \left(\frac{1+n}{n}\right)^{\frac{n}{1+n}} \quad \text{and} \quad C_2 = \frac{2n^2}{(1+n)(2n+1)}C_1^2 - C_1^{\frac{n-1}{n}}.$$

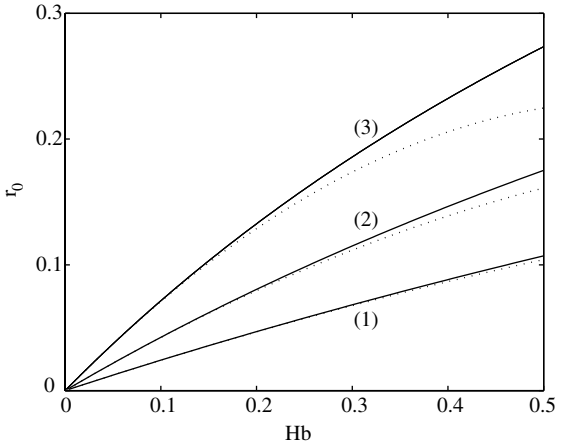

Fig. 3. Dimensionless radius of the plug zone as function of Hb. (1) $n = 1$; (2) $n = 0.5$; (3) $n = 0.1$. The dashed line show expansion to $r_0(Hb)$ valid for small Hb.

Fig. 3 shows the asymptotic expressions $r_0(Hb)$ for $Hb < 1$, plotted against the numerical solution of Eq. (12) for three values of n. It is observed that the limit of validity of Eq. (13) decreases with increasing the shear thinning of the fluid.

4. Asymptotic analysis

An asymptotic analysis was previously used by Nouar et al. [20] to study the laminar mixed convection for power law fluids in the thermal entrance region of an annular duct. The results obtained by this method were in good agreement with the experimental ones (e.g. see Fig. 16 in Ref. [20]). Encouraged by this, the procedure is extended here to the Herschel–Bulkley fluids.

For $Pe \to \infty$, the temperature variations are confined to a thin region (thermal boundary layer) adjacent to the wall. Thus it is possible to resort to an asymptotic solution. Two regions are then distinguished: the internal region (thermal boundary layer) and the external region which contains the pseudo-plug zone. The characteristic scale of the internal region which satisfies the least degeneracy principle [21,22] is $\delta = Pe^{-1/3}$. The solution can then be written as an expansion into series in δ.

- At the leading order in δ, we have $\theta \sim 0$ in the external zone. In other words, the external zone "does not see" the wall heating and the temperature variations are confined only in the internal zone.
  - If the rheological parameters and the thermophysical properties are independent of the temperature, i.e., $Gr = Pn = 0$, the temperature distribution in the internal zone is given by the Lévêque solution (Eq. (33)). The velocity field as well as the axial pressure gradient are the same as those at the entrance section, $z = 0$. Indeed, if $Gr = Pn = 0$, the flow field will be not modified along all the heating zone since it is assumed fully developed at $z = 0$.
  - When the density and the consistency are thermo-dependent, we still have $\theta \sim 0$ in the external zone. As indicated above, at the leading order in δ, the external zone "does not see" any effect of the heating wall. The velocity field is not disturbed and is identical to that at the inlet. In the internal zone, the temperature variation will generate secondary flows. Near the entrance section, the thermal boundary layer is very thin and the intensity, $\mathscr{I}$, of these secondary flows is weak. Formally, $\mathscr{I}$ can be written as a function of two small parameters ε_1 and ε_2, defined later in the analysis, which represent the thermo-dependency effect of $K^*(T^*)$ and $\rho(T^*)$ respectively. The velocity field corresponding to the secondary flows can be first calculated using the temperature distribution evaluated in the situation $Gr = Pn = 0$, and then improved, taking into account the modification of the temperature distribution by these secondary flows.
- At the first order in δ, the calculations are too complex, and only qualitative results are provided for the external zone. It is shown that we still have $\theta \sim 0$, and the modification of the velocity field is induced by the secondary flows developed in the internal zone.

The above analysis summarizes the asymptotic developments performed in this section.

Zeroth order in the external region: In the external region, the flow solution is obtained by expanding the dependent variables into series in δ

$$u^{\text{ext}} \sim u_0^{\text{ext}} + \delta u_1^{\text{ext}} + \cdots, \tag{15}$$

$$v^{\text{ext}} \sim v_0^{\text{ext}} + \delta v_1^{\text{ext}} + \cdots, \tag{16}$$

$$w^{\text{ext}} \sim w_0^{\text{ext}} + \delta w_1^{\text{ext}} + \cdots, \tag{17}$$

$$P^{\text{ext}} \sim P_0^{\text{ext}} + \delta P_1^{\text{ext}} + \cdots, \tag{18}$$

$$\theta^{\text{ext}} \sim \theta_0^{\text{ext}} + \delta \theta_1^{\text{ext}} + \cdots, \tag{19}$$

where $u_1^{\text{ext}}, v_1^{\text{ext}}, w_1^{\text{ext}}, P_1^{\text{ext}}$ and θ_1^{ext} are function of the two parameters ε_1 and ε_2 as explained above.

By substituting (15)–(19) into the full problem (3)–(5) and taking the limit as $Pe \to \infty$ the equations corresponding to the zeroth order solution $u_0^{\text{ext}}, v_0^{\text{ext}}, w_0^{\text{ext}}, P_0^{\text{ext}}$ and θ_0^{ext} are derived. The solution which satisfy the fully developed axial velocity profile and uniform temperature at the inlet are just these undisturbed inlet conditions.

$$\theta_0^{\text{ext}} = 0; \quad v_0^{\text{ext}} = 0; \quad \frac{\partial P_0^{\text{ext}}}{\partial r} = 0; \quad w_0^{\text{ext}} = 0, \tag{20}$$

$$u_0^{\text{ext}} = U_{\text{fd}}(r); \quad \frac{\partial P_0^{\text{ext}}}{\partial z} = \left(\frac{\mathrm{d}P}{\mathrm{d}z}\right)_{\text{fd}}. \tag{21}$$

The subscript "fd" means fully developed flow.

Zeroth order boundary layer: Near the pipe wall, the heat conduction normal to the wall becomes important. The radial co-ordinate r is stretched to reflect this physical fact. Accordingly and as in classical boundary layer, the following inner variables are introduced:

$$r = 1 - \delta\bar{r}, \quad u = \delta\hat{u}, \quad v = -\delta^2\hat{v}, \quad w = \delta\hat{w}. \tag{22}$$

The variation of the consistency K^* with the temperature is expanded using a Taylor series at the reference temperature T_{e}^*.

$$K^* = K_{\text{e}}^*\left[1 - \varepsilon_2\theta + \frac{\varepsilon_2^2}{2}\theta^2 + \mathrm{O}\left(\varepsilon_2^3\right)\right] = K_{\text{e}}^* K,$$

with

$$\varepsilon_2 = \frac{b\Phi^* R^*}{\lambda Pe^{1/3}} = \frac{P_n}{Pe^{1/3}}.$$

In the thermal entrance region, the parameter ε_2 is more relevant than Pn to account for the thermo-dependency of K. Indeed, it can be shown that ε_2 is the characteristic scale of the relative variation of the consistency between the wall and the edge of the thermal boundary layer: $(K_{\text{e}}^* - K_{\text{w}}^*)/K_{\text{e}}^* = \mathrm{O}(\varepsilon_2)$.

Expressions (22) are combined with the governing equations (3)–(5) and the solution is expanded into series in δ. Finally, after retaining the leading order terms, that is the zeroth order solution, we obtain:

$$\frac{\partial\hat{v}}{\partial\bar{r}} + \frac{\partial\hat{w}}{\partial\phi} + \frac{\partial\hat{u}}{\partial z} = 0, \tag{23}$$

$$\frac{1}{Pr}\left[\hat{v}\frac{\partial\hat{w}}{\partial\bar{r}} + \hat{w}\frac{\partial\hat{w}}{\partial\phi} + \hat{u}\frac{\partial\hat{w}}{\partial z}\right] = \varepsilon_1\theta\sin\phi + \frac{\partial}{\partial\bar{r}}\left[\mu_{\text{a0}}\frac{\partial\hat{w}}{\partial\bar{r}}\right], \tag{24}$$

$$\frac{1}{Pr}\left[\hat{v}\frac{\partial\hat{u}}{\partial\bar{r}} + \hat{w}\frac{\partial\hat{u}}{\partial\phi} + \hat{u}\frac{\partial\hat{u}}{\partial z}\right] = \frac{\partial}{\partial\bar{r}}\left[\mu_{\text{a0}}\frac{\partial\hat{u}}{\partial\bar{r}}\right], \tag{25}$$

$$\hat{v}\frac{\partial\theta}{\partial\bar{r}} + \hat{w}\frac{\partial\theta}{\partial\phi} + \hat{u}\frac{\partial\theta}{\partial z} = \frac{\partial^2\theta}{\partial\bar{r}^2}, \tag{26}$$

where

$$Pr = \frac{K_{\text{e}}^*(U_d^*)^{n-1}C_p}{(R^*)^{n-1}\lambda}; \quad \mu_{\text{a0}} = \frac{Hb}{(4D_{\text{II0}})^{1/2}} + K(4D_{\text{II0}})^{(n-1)/2};$$

$$D_{\text{II0}} = \frac{1}{4}\left[\left(\frac{\partial\hat{u}}{\partial\bar{r}}\right)^2 + \left(\frac{\partial\hat{w}}{\bar{r}}\right)^2\right] \quad \text{and} \quad \varepsilon_1 = \frac{Gr}{RePe^{2/3}}.$$

Pr is the generalized Prandtl number and μ_{a0} is the apparent viscosity at the zeroth order in δ. The perturbation parameter ε_1 is the characteristic scale of the ratio of the azimuthal velocity to the axial velocity inside the thermal boundary layer: $w/u = \mathrm{O}(\varepsilon_1)$.

It is clear that ε_1 and ε_2 are two regular perturbation parameters. The solution is obtained using double series in ε_1 and ε_2:

$$A \sim A_{00} + \varepsilon_1 A_{10} + \varepsilon_2 A_{01} + \varepsilon_1\varepsilon_2 A_{11} + \varepsilon_1^2 A_{20} + \varepsilon_2^2 A_{02} + \ldots, \tag{27}$$

where A stands for $\hat{u}, \hat{v}, \hat{w}$ and θ. The product $\varepsilon_1\varepsilon_2$ traduces the modification of the azimuthal velocity by the thermo-dependency of K: $\hat{w}_{\text{th}} - \hat{w}_n\text{th} = \mathrm{O}(\varepsilon_1\varepsilon_2)$. The subscripts th and nth mean thermo-dependent and non-thermo-dependent respectively. In the following analysis, it is necessary to introduce a hierarchy between ε_1 and ε_2. For this, it is assumed that there is a parameter $\varsigma > 0$ such that $\varepsilon_1 = (\varepsilon_2)^{\varsigma}$. Three cases can be considered: $\varsigma > 1$, $\varsigma < 1$ and $\varsigma = 1$, depending on whether the effect of $K^*(T^*)$ is more important, or less important or of the same order as that of $\rho(T^*)$. Based on the different rheological tests performed in our laboratory [14], only the situation where $\varsigma > 1$ ($\varepsilon_1 < \varepsilon_2$) is considered. However, for $\varsigma \geqslant 2$, the product $\varepsilon_1\varepsilon_2 \leqslant \varepsilon_2^3$ and $\varepsilon_1 \leqslant \varepsilon_2^2$. Here, the study is restricted to the case where $1 < \varsigma < 2$. Homogeneous solutions are then determined [23] leading to the following relations:

$$\hat{u} \sim (az)^{1/3}\eta\Pi\varphi_{\text{new}} + \varepsilon_1(az)^2 H'_{10}\cos\phi + \varepsilon_2(az)^{2/3}H'_{01} + \varepsilon_2^2(az)H'_{02} + \varepsilon_1\varepsilon_2(az)^{7/3}H'_{11}\cos\phi + \cdots, \tag{28}$$

$$\hat{v} \sim \varepsilon_1(az)^{4/3}\Psi_{10}\cos\phi + \varepsilon_2\Psi_{01} + \varepsilon_2^2(az)^{2/3}\Psi_{02} + \varepsilon_1\varepsilon_2(az)^{5/3}\Psi_{11}\cos\phi + \cdots, \tag{29}$$

$$\hat{w} \sim \varepsilon_1(az)F'_{10}\sin\phi + \varepsilon_1\varepsilon_2(az)^{4/3}F'_{11}\sin\phi + \cdots, \tag{30}$$

$$\theta \sim (az)^{1/3}G_{00} + \varepsilon_1(az)^2 G_{10}\cos\phi + \varepsilon_2(az)^{2/3}G_{01} + \varepsilon_2^2(az)G_{02} + \varepsilon_1\varepsilon_2(az)^{7/3}G_{11}\cos\phi + \cdots, \tag{31}$$

The functions H_{ij}, Ψ_{ij}, F_{ij} and G_{ij} $(i,j = 0,1)$ depend only on $\eta : \eta = \bar{r}/(az)^{1/3}$ and $a = 9/(\Pi\varphi_{\text{new}})$. They traduce the distribution of the velocity and the temperature inside the thermal boundary layer. One can observe that $\hat{u}$, $\hat{v}$, $\hat{w}$ and θ depend not only on the similarity variable η, but also on the axial position because the wall temperature varies along the heating zone, as a uniform heat flux is imposed. Substituting expressions (28)–(31) into Eqs. (23)–(26) and collecting the terms of zero order, which correspond to the situation of forced convection with $K = \text{const.}$, we obtain:

$$G''_{00} + 3\eta^2 G'_{00} - 3\eta G_{00} = 0. \tag{32}$$

The boundary conditions are

$$G'_{00} = -1 \quad \text{at } \eta = 0; \quad G_{00} \to 0 \quad \text{as } \eta \to \infty.$$

The solution is given by

$$G_{00}(\eta) = \frac{2}{3\Gamma(5/3)}\mathrm{e}^{-\eta^3} - \eta\left[1 - \frac{2}{\Gamma(5/3)}\int_0^\eta \xi \mathrm{e}^{-\xi^3}\,\mathrm{d}\xi\right]. \quad (33)$$

Eq. (33) represents the temperature profile in the thermal boundary layer, in the situation of constant physical properties, linear velocity profile and no curvature effect. It is known in the literature as the Lévêque solution [24]. The value of G_{00} at the wall is useful and is given by $G_{00}(0) = 0.738488$.

The terms of order ε_1, which correspond to the perturbation of forced convection solution by the buoyancy force with $K = \text{const.}$, lead to:

$$\frac{\varphi^{n-1}}{1-r_0}F'''_{10} + \frac{3}{Pr}[\eta^2 F''_{10} - 3\eta F'_{10}] = -G_{00}, \quad (34)$$

$$n\varphi^{n-1}H'''_{10} + \frac{3}{Pr}[\eta^2 H''_{10} - 7\eta H'_{10} + 7H_{10}] = -\frac{9}{aPr}F_{10}, \quad (35)$$

$$G''_{10} + 3\eta^2 G'_{10} - 18\eta G_{10} = \left[\Psi_{10}G'_{00} + \frac{a}{3}H'_{10}(G_{00} - \eta G'_{00})\right], \quad (36)$$

$$\Psi_{10}(\eta) = \frac{a}{3}\eta H'_{10}(\eta) - \frac{7a}{3}H_{10}(\eta) - F_{10}. \quad (37)$$

The terms of order ε_2 correspond to the perturbation of forced convection by the thermo-dependency of K:

$$n\varphi^{n-1}H'''_{01} + \frac{3}{Pr}[\eta^2 H''_{01} - 3\eta H'_{01} + 3H_{01}] = \frac{9}{a}\varphi^{n-1}G'_{00}, \quad (38)$$

$$G''_{01} + 3\eta^2 G'_{01} - 6\eta G_{01} = \frac{a}{3}[H'_{01}G_{00} - 3H_{01}G'_{00}], \quad (39)$$

$$\Psi_{01} = \frac{a}{3}(\eta H'_{01} - 3H_{01}). \quad (40)$$

The terms of order ε_2^2 represent a perturbation of second order of forced convection solution by the thermo-dependency of K, with $\rho = \text{const}$. We have:

$$n\varphi^{n-1}H'''_{02} + \frac{3}{Pr}[\eta^2 H''_{02} - 4\eta H'_{02} + 4H_{02}] = -\frac{9}{a}\varphi^{n-1}[G_{00}G'_{00} - G'_{01}] + n\varphi^{n-1}[G'_{00}H''_{01} + G_{00}H'''_{01}] + \frac{a}{3Pr}[2H'^2_{01} - 3H_{01}H''_{01}] + \frac{2Hb}{\varphi^2}H''_{01}H'''_{01} - 2\frac{n-1}{\varphi}\varphi^{n-1}H''_{01}H'''_{01}, \quad (41)$$

$$G''_{02} + 3\eta^2 G'_{02} - 9\eta G_{02} = \frac{a}{3}[H'_{02}G_{00} - 4H_{02}G'_{00}], \quad (42)$$

$$\Psi_{02} = \frac{a}{3}(\eta H'_{02} - 4H_{02}). \quad (43)$$

From the terms of order $\varepsilon_1\varepsilon_2$ which correspond to mixed convection with thermo-dependent consistency, we have:

$$n\varphi^{n-1}H'''_{11} + \frac{3}{Pr}[\eta^2 H''_{11} - 8\eta H'_{11} + 8H_{11}] = \frac{9}{a}\varphi^{n-1}G'_{10} + n\varphi^{n-1}\frac{\mathrm{d}}{\mathrm{d}\eta}(G_{00}H''_{10}) + \frac{1}{Pr}\left[\Psi_{10}H''_{01} - \frac{a\eta}{3}H'_{10}H''_{01} + \Psi_{01}H''_{10} - \frac{a\eta}{3}H'_{01}H''_{10}\right] + \frac{1}{Pr}\left[\frac{8a}{3}H'_{01}H'_{10} - \frac{9}{a}F_{11}\right] + \frac{a^2}{27}Hb\frac{\mathrm{d}}{\mathrm{d}\eta}[H''_{01}H''_{10}] - 3\frac{n-1}{\varphi}\varphi^{n-1}\frac{\mathrm{d}}{\mathrm{d}\eta}[H''_{10}H''_{01}], \quad (44)$$

$$\frac{\varphi^{n-1}}{1-r_0}F'''_{11} + \frac{3}{Pr}[\eta^2 F''_{11} - 4\eta F'_{11}] = -G_{01} + \frac{a}{Pr}[H'_{01}F'_{10} - H_{01}F''_{10}] + \frac{a}{9}\frac{r_0}{1-r_0}\frac{\mathrm{d}}{\mathrm{d}\eta}(F''_{10}H''_{01}) + \varphi^{n-1}\frac{\mathrm{d}}{\mathrm{d}\eta}(G_{00}F''_{10}), \quad (45)$$

$$G''_{11} + 3\eta^2 G'_{11} - 21\eta G_{11} = [\Psi_{10}G'_{01} + \Psi_{01}G'_{10} + \Psi_{11}G'_{00}] + \frac{a}{3}[H'_{01}(6G_{10} - \eta G'_{10}) + H'_{10}(2G_{01} - \eta G'_{01})] + \frac{a}{3}H'_{11}[G_{00} - \eta G'_{00}], \quad (46)$$

$$\Psi_{11} = -F_{11} + \frac{a}{3}(\eta H'_{11} - 8H_{11}). \quad (47)$$

With the following boundary conditions:

$$\begin{cases} F_{10} = F'_{10} = H_{10} = H'_{10} = G'_{10} = 0 \text{ at } \eta = 0, \\ F'_{10} = G_{10} = H''_{10} \to 0 \text{ as } \eta \to \infty, \end{cases}$$
$$\begin{cases} H_{01} = H'_{01} = G'_{01} = 0 \text{ at } \eta = 0, \\ H''_{01} = G_{01} \to 0 \text{ as } \eta \to \infty, \end{cases}$$
$$\begin{cases} H_{02} = H'_{02} = G'_{02} = 0 \text{ at } \eta = 0, \\ H''_{02} = G_{02} \to 0 \text{ as } \eta \to \infty, \end{cases}$$
$$\begin{cases} F'_{11} = H'_{11} = G'_{11} = 0 \text{ at } \eta = 0, \\ F'_{11} = H''_{11} = G_{11} \to 0 \text{ as } \eta \to \infty. \end{cases}$$

The set of ordinary differential equations (34)–(47) are integrated numerically using a fourth order Runge–Kutta method with shooting.

First order core flow: Substituting expressions (15)–(19) into the dimensionless governing equations, we obtain:

$$\frac{1}{r}\frac{\partial}{\partial r}(rv_1^{\text{ext}}) + \frac{1}{r}\frac{\partial w_1^{\text{ext}}}{\partial \phi} + \frac{\partial u_1^{\text{ext}}}{\partial z} = 0, \quad (48)$$

$$u_0^{\text{ext}}\frac{\partial v_1^{\text{ext}}}{\partial z} = -\frac{\partial P_1^{\text{ext}}}{\partial r} - \varepsilon_1\theta_1^{\text{ext}}\cos(\phi) + A_r, \quad (49)$$

$$u_0^{\text{ext}}\frac{\partial w_1^{\text{ext}}}{\partial z} = -\frac{1}{r}\frac{\partial P_1^{\text{ext}}}{\partial \phi} + \varepsilon_1\theta_1^{\text{ext}}\sin(\phi) + A_\phi, \quad (50)$$

$$v_1^{\text{ext}}\frac{\mathrm{d}u_0^{\text{ext}}}{\mathrm{d}r}+u_0^{\text{ext}}\frac{\partial u_1^{\text{ext}}}{\partial z}=-\frac{\partial P_1^{\text{ext}}}{\partial z}+A_z, \tag{51}$$

$$\frac{\partial\theta_1^{\text{ext}}}{\partial z}=0, \tag{52}$$

where A_r, A_ϕ and A_z are the first order terms in an expansion of the radial, azimuthal and axial component respectively of $\nabla\cdot[\boldsymbol{\tau}(\boldsymbol{u}_0^{\text{ext}}+\delta\boldsymbol{u}_1^{\text{ext}})-\boldsymbol{\tau}(\boldsymbol{u}_0^{\text{ext}})]$. Using Eqs. (6), (8), (15)–(17) and (19)–(21), A_r, A_ϕ and A_z may be recast in terms of gradients of velocity components. For instance, we have:

$$A_\phi=\frac{1}{Re}\mu_{\text{a0}}^{\text{ext}}\left[\Delta w_1^{\text{ext}}+\frac{2}{r^2}\frac{\partial v_1^{\text{ext}}}{\partial\phi}-\frac{w_1^{\text{ext}}}{r^2}\right]+\frac{1}{Re}\frac{\mathrm{d}}{\mathrm{d}r}(\mu_{\text{a0}}^{\text{ext}})\left[\frac{1}{r}\frac{\partial v_1^{\text{ext}}}{\partial\phi}+\frac{\partial w_1^{\text{ext}}}{\partial r}-\frac{w_1^{\text{ext}}}{r}\right],$$

where

$$\mu_{\text{a0}}^{\text{ext}}=\frac{Hb}{|\mathrm{d}u_0^{\text{ext}}/\mathrm{d}r|}+\left|\frac{\mathrm{d}u_0^{\text{ext}}}{\mathrm{d}r}\right|^{n-1}.$$

The solution of Eq. (52) is $\theta_1^{\text{ext}}=0$. The temperature of the external zone, up to this order, is still not changed and is equal to the inlet temperature. Therefore, there is no buoyancy force acting on the fluid in the external zone. Eqs. (49) and (50) can then be simplified in this sense. Actually, Eqs. (48)–(51) traduce the deceleration of the axial flow due to the motion of the fluid particles towards the heated wall, and the downward cold stream due to the displacement effect of the dynamical boundary layer associated to the secondary flow induced by the buoyancy force in the thermal boundary layer. Within the overlap zone between the internal and external regions, the corresponding solutions should "match", in accordance with the requirement of the method of singular perturbation [21]. For example, in the situation of forced convection with $K^*(T^*)$, we have

$$\lim_{r\to 1}u_1^{\text{ext}}=\delta\lim_{\eta\to\infty}\hat{u}=\delta[\varepsilon_2(az)^{2/3}\alpha_1+\cdots],\quad\text{where }\alpha_1=\lim_{\eta\to\infty}H'_{01}. \tag{53}$$

Similar equations can be derived for v_1^{ext} and w_1^{ext}. Finally, the solution of Eqs. (48)–(51) are written in the form:

$$u_1^{\text{ext}}\sim\varepsilon_1u_{11}^{\text{ext}}\cos(\phi)+\varepsilon_2u_{12}^{\text{ext}}+\varepsilon_2^2u_{13}^{\text{ext}}+\varepsilon_1\varepsilon_2u_{14}^{\text{ext}}\cos(\phi), \tag{54}$$

$$v_1^{\text{ext}}\sim\varepsilon_1v_{11}^{\text{ext}}\cos(\phi)+\varepsilon_2v_{12}^{\text{ext}}+\varepsilon_2^2v_{13}^{\text{ext}}+\varepsilon_1\varepsilon_2v_{14}^{\text{ext}}\cos(\phi), \tag{55}$$

$$w_1^{\text{ext}}\sim\varepsilon_1w_{11}^{\text{ext}}\sin(\phi)+\varepsilon_1\varepsilon_2w_{14}^{\text{ext}}\sin(\phi), \tag{56}$$

$$P_1^{\text{ext}}\sim\varepsilon_1P_{11}^{\text{ext}}\cos(\phi)+\varepsilon_2P_{12}^{\text{ext}}+\varepsilon_2^2P_{13}^{\text{ext}}+\varepsilon_1\varepsilon_2P_{14}^{\text{ext}}\cos(\phi). \tag{57}$$

5. Results and discussion

5.1. Forced convection with thermo-dependent consistency

As explained before, the decrease of the consistency K^* with increasing T^* induces a radial motion of fluid particles towards the heated wall. The axial flow is accelerated in the thermal boundary layer. At the first order in ε_2, the redistribution of the velocities and temperatures is governed by Eqs. (38)–(40). It is important to note that this redistribution depends only on the Prandtl number, the flow behavior index and on the dimensionless wall shear rate, φ. The numerical results for the functions $G_{00}, H'_{01}, \Psi_{01}$ and G_{01} are plotted respectively in Fig. 4(a)–(d) for $n=1$, $Pr=200$ and five values of r_0: 0, 0.2, 0.4, 0.6 and 0.8. For a fixed value of r_0, the effect of the flow behavior index, n, on the flow reorganization and temperature modification is represented in Fig. 5.

Remark. Fig. 4(c) and (d) shows that for a large Prandtl number, the dimension of the plug zone has no significant effect on $\Psi_{01}(\eta)$ and $G_{01}(\eta)$.

Concerning the physical meaning of the functions H'_{01}, Ψ_{01} and G_{01}, they represent, for a given axial position, the increase of the axial velocity, the radial motion of the fluid particles and the decrease of the temperature inside the internal region, respectively.

Using the first order term in ε_2 in Eq. (29), the radial velocity of the fluid particles inside the thermal boundary layer is $v\sim-\delta^2\varepsilon_2\Psi_{01}$. The intensity of this secondary flow can be represented by v calculated at $\eta=\eta_0=|G'_{00}(0)\times G_{00}(0)|$:

$$v(\eta_0)\sim-\frac{Pn}{Pe}\Psi_{01}(\eta_0). \tag{58}$$

Finally, for $0\leqslant r_0\leqslant 0.8$, $0.4\leqslant n\leqslant 1$, the numerical results show that $\Psi_{01}(\eta_0)$ can be described by $-0.53/n$ with a relative error less than 4%, when $Pr\geqslant 100$. Then, in this case, one can write:

$$v(\eta_0)\approx\frac{0.53}{n}\frac{Pn}{Pe}. \tag{59}$$

The intensity of the secondary flow increases with the shear thinning of the fluid (Fig. 5(a)).

Concerning the acceleration of the axial flow, the asymptotic solution gives:

$$\frac{\partial\hat{u}}{\partial z}\sim\varepsilon_2\frac{a}{3(az)^{1/3}}[2H'_{01}-\eta H''_{01}]+\cdots \tag{60}$$

Thus, the flow is quickly accelerated near the entrance, then, the acceleration declines downstream as $(az)^{-1/3}$. The modification of the wall axial velocity gradient along the heated zone can be characterized by the ratio Π' as:

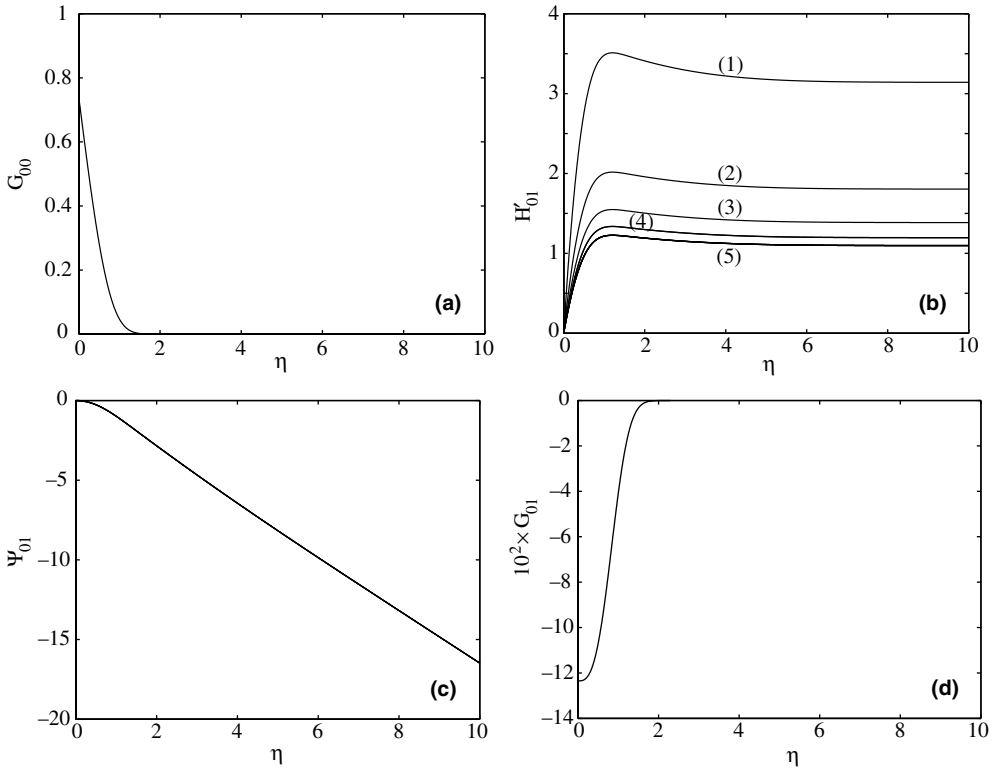

Fig. 4. Functions: (a) $G_{00}(\eta)$; (b) $H'_{01}(\eta)$; (c) $\Psi_{01}(\eta)$ and (d) $G_{01}(\eta)$ for $Pr = 200$ and $n = 1$. (1) $r_0 = 0$; (2) $r_0 = 0.2$; (3) $r_0 = 0.4$; (4) $r_0 = 0.6$; (5) $r_0 = 0.8$.

$$\Pi' = \frac{|\,\partial u/\partial r|_{r=1,z}}{|\,\partial u/\partial r|_{r=1,z=0}}.$$

Near the entrance section and for a large Prandtl number, we have:

$$\Pi' \sim 1 + \frac{Pn}{n}\left[\frac{9X^+}{\Pi\varphi_{\text{new}}}\right]^{1/3} G_{00}(0) + \cdots \tag{61}$$

The above equation shows clearly that for a yield stress fluid, the increase of the wall axial velocity gradient, due to the decrease of K near the heated wall, is less important when Π and then Hb is high. The shear thinning ($n \leqslant 1$), effect is more complex, since on one hand it contributes to increase the wall shear rate, i.e. Π, and on the other hand, it enhances the thermo-dependency phenomenon through the term Pn/n. However, calculations performed for $0.3 \leqslant n \leqslant 1$ show that $n\Pi^{1/3} \leqslant 1$ and Π' increases with the shear thinning.

As far as the local axial shear stress is concerned, it is given by

$$\tau^*_{rz} = \operatorname{sgn}\left(\frac{\partial u^*}{\partial r^*}\right)\tau^*_{\text{y}} + K^*\left|\frac{\partial u^*}{\partial r^*}\right|^{n-1}\frac{\partial u^*}{\partial r^*}. \tag{62}$$

The ($K(\theta)$) variation effect on the axial shear stress at the wall can be illustrated by the ratio:

$$\frac{\tau^*_{rz,\text{th}}}{\tau^*_{rz,n\text{th}}} \sim 1 - \varepsilon_2(1-r_0)(az)^{1/3}\left(G_{00} - \frac{nH''_{01}}{\varphi}\right) - \varepsilon_2^2(1-r_0) \times (az)^{2/3}\left(\frac{G_{00}^2}{2} + G_{00}\left(\frac{nH''_{01}}{\varphi} - G_{00}\right) + G_{01} - \frac{nH''_{02}}{\varphi}\right). \tag{63}$$

In Eq. (63), the different functions are evaluated at $\eta = 0$. For a large Prandtl number, using Eqs. (38) and (41), the relation (63) can be reduced to:

$$\frac{\tau^*_{rz,\text{th}}}{\tau^*_{rz,n\text{th}}} \sim 1 + \left(\frac{Pn}{n}\right)^2\left[\frac{9X^+}{\Pi\varphi_{\text{new}}}\right]^{2/3} G_{00}^2(0)(1 - n(1-r_0)). \tag{64}$$

The modification of the axial shear stress due to $K(\theta)$ variation is of second order in ε_2.

Concerning the heat transfer coefficient, the Nusselt number is defined by $Nu = [\delta \times \theta(\eta = 0)]^{-1}$. The asymptotic solution leads to:

$$\frac{Nu_{\text{th}}}{Nu_{n\text{th}}} \sim \frac{G_{00}(0)}{G_{00}(0) + \varepsilon_2(az)^{1/3}G_{01}(0)}. \tag{65}$$

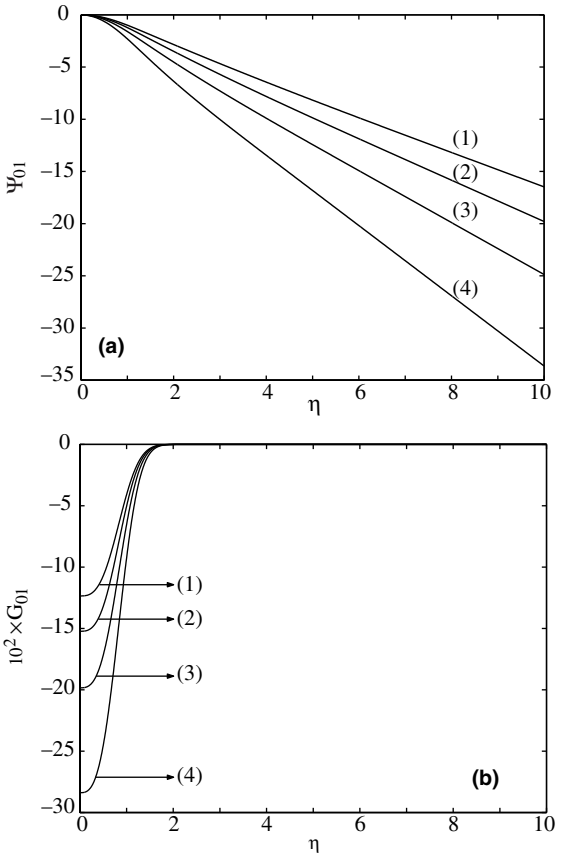

Fig. 5. Functions: (a) $\Psi_{01}(\eta)$ and (b) $G_{01}(\eta)$ for $Pr = 200$; $r_0 = 0.4$ and different flow behavior index, n. (1) $n = 1$; (2) $n = 0.8$; (3) $n = 0.6$; (4) $n = 0.4$.

For large Pr, the previous relation may be reduced to:

$$\frac{Nu_{\mathrm{th}}}{Nu_{n\mathrm{th}}} \sim 1 - \frac{Pn}{n}\frac{G_{01}(0)_{\mathrm{new}}}{G_{00}(0)}\left(\frac{9X^+}{\Pi\varphi_{\mathrm{new}\,t}}\right)^{1/3}, \tag{66}$$

with $G_{01}(0)_{\mathrm{new}} = -0.123$ and $Nu_{n\mathrm{th}} = \frac{1}{G_{00}(0)}\left(\frac{9X^+}{\Pi\varphi_{\mathrm{new}}}\right)^{-1/3}$.

The relation (66) shows that the Nusselt number increases with Pn and this increase is more significant when the fluid is shear thinning or the wall shear rate is low. This result is consistent with the experimental data given by Naïmi et al. [13] and Nouar et al. [15].

As far as the flow in the external zone is concerned, we follow the procedure described by Walton and Bittleston [25] then Balmforth and Craster [26] and Frigaard and Ryan [27]. Outside the pseudo-yield surface, using the expansion into series (15)–(17), the components of the rate-of-strain tensor take the form

$$D_{zz}^{\mathrm{ext}} \sim \delta D_{zz1}^{\mathrm{ext}} + \cdots, \quad D_{rr}^{\mathrm{ext}} \sim \delta D_{rr1}^{\mathrm{ext}} + \cdots,$$
$$D_{rz}^{\mathrm{ext}} \sim D_{rz0}^{\mathrm{ext}} + \delta D_{rz1}^{\mathrm{ext}} + \cdots \tag{67}$$

and

$$D_{\mathrm{II}}^{\mathrm{ext}} \sim |D_{rz0}^{\mathrm{ext}}| + \delta D_{\mathrm{II}1}^{\mathrm{ext}} + \cdots, \tag{68}$$

where

$$D_{zz1}^{\mathrm{ext}} = \frac{\partial u_1^{\mathrm{ext}}}{\partial z}, \quad D_{rr1}^{\mathrm{ext}} = \frac{\partial v_1^{\mathrm{ext}}}{\partial r}, \quad D_{rz0}^{\mathrm{ext}} = \frac{1}{2}\frac{\mathrm{d}u_0^{\mathrm{ext}}}{\mathrm{d}r},$$
$$D_{rz1}^{\mathrm{ext}} = \frac{1}{2}\left(\frac{\partial u_1^{\mathrm{ext}}}{\partial r} + \frac{\partial v_1^{\mathrm{ext}}}{\partial z}\right). \tag{69}$$

It follows that the stresses take the form

$$\tau_{rr}^{\mathrm{ext}} \sim \delta\tau_{rr1}^{\mathrm{ext}} + \cdots, \quad \tau_{zz}^{\mathrm{ext}} \sim \delta\tau_{zz1}^{\mathrm{ext}} + \cdots,$$
$$\tau_{rz}^{\mathrm{ext}} \sim \tau_{rz0}^{\mathrm{ext}} + \delta\tau_{rz1}^{\mathrm{ext}} + \cdots, \tag{70}$$

where

$$\tau_{zz1}^{\mathrm{ext}} = \frac{2}{Re}\left[\frac{Hb}{2|D_{rz0}|} + (2|D_{rz0}|)^{n-1}\right]D_{zz1}^{\mathrm{ext}},$$
$$\tau_{rr1}^{\mathrm{ext}} = \frac{2}{Re}\left[\frac{Hb}{2|D_{rz0}|} + (2|D_{rz0}|)^{n-1}\right]D_{rr1}^{\mathrm{ext}},$$
$$\tau_{rz0} = -\frac{Hb}{Re}\frac{r}{r_0}, \quad \tau_{rz1}^{\mathrm{ext}} = \frac{2}{Re}\left[\frac{Hb}{2|D_{rz0}|} + (2|D_{rz0}|)^{n-1}\right]D_{rz1}^{\mathrm{ext}}. \tag{71}$$

It is clear that $\tau_{zz1}^{\mathrm{ext}}$ and $\tau_{rr1}^{\mathrm{ext}}$ diverge at the pseudo-yield surface where $D_{rz0}^{\mathrm{ext}} = 0$. As explained by Balmforth and Craster [26], this divergence is due to the fact that the asymptotic expansion of the constitutive equation is not uniform.

In the pseudo-plug region, the velocity components may be expanded as:

$$u^{\mathrm{pp}} \sim u_0^{\mathrm{pp}} + \delta u_1^{\mathrm{pp}} + \cdots \quad \text{and} \quad v^{\mathrm{pp}} \sim \delta v_1^{\mathrm{pp}} + \cdots \tag{72}$$

then

$$D_{zz}^{\mathrm{pp}} \sim \delta\frac{\partial u_1^{\mathrm{pp}}}{\partial z} + \cdots, \quad D_{rr}^{\mathrm{pp}} \sim \delta\frac{\partial v_1^{\mathrm{pp}}}{\partial r},$$
$$D_{rz}^{\mathrm{pp}} \sim \frac{1}{2}\delta\left(\frac{\partial u_1^{\mathrm{pp}}}{\partial r} + \frac{\partial v_1^{\mathrm{pp}}}{\partial z}\right) + \cdots \tag{73}$$

The superscript "pp" means pseudo-plug. Combining the above relations, the second invariant of the strain-rate tensor can be written as $D_{\mathrm{II}}^{\mathrm{pp}} \sim \delta D_{\mathrm{II}1}^{\mathrm{pp}} + \cdots$. Concerning the stresses, we have at the leading order:

$$\tau_{zz0}^{\mathrm{pp}} = \frac{2}{Re}\left[\frac{Hb}{D_{\mathrm{II}1}^{\mathrm{pp}}}\right]\frac{\partial u_1^{\mathrm{pp}}}{\partial z}, \quad \tau_{rr0}^{\mathrm{pp}} = \frac{2}{Re}\left[\frac{Hb}{D_{\mathrm{II}1}^{\mathrm{pp}}}\right]\frac{\partial v_1^{\mathrm{pp}}}{\partial r}, \tag{74}$$

$$\tau_{rz0}^{\mathrm{pp}} = \frac{1}{Re}\left[\frac{Hb}{D_{\mathrm{II}1}^{\mathrm{pp}}}\right]\left[\frac{\partial u_1^{\mathrm{pp}}}{\partial r} + \frac{\partial v_1^{\mathrm{pp}}}{\partial z}\right] \quad \text{and}$$
$$\tau_{\mathrm{II}}^{\mathrm{pp}} = \left(\frac{Hb}{Re}\right)^2 + \cdots \tag{75}$$

Thus, within the pseudo-plug, the stress exceeds the yield stress. The relation $\tau_{rz0}^{\mathrm{ext}} = -(Hb/Re)(r/r_0)$ is also satisfied within the pseudo-plug: $\tau_{rz0}^{\mathrm{pp}} = -(Hb/Re)(r/r_0)$. Therefore $\tau_{zz0}^{\mathrm{pp}} \mapsto 0$ and $\tau_{rr0} \mapsto 0$ as $r \mapsto r_0$. Along the axis, we have $\tau_{rz0}^{\mathrm{pp}} = 0$ and $(\tau_{rr0}^{\mathrm{pp}})^2 = (\tau_{zz0}^{\mathrm{pp}})^2 = (Hb/Re)^2$.

5.2. Mixed convection with constant consistency

Due to the decrease of the density with temperature, the warmer fluid moves upward along the heated wall and the cooler fluid moves downward in the external zone. This secondary flow is described by the azimuthal velocity $w \sim \delta\varepsilon_1 azF'_{10}\sin\phi$. The numerical results of F'_{10} are shown in Figs. 6(a) and 7(a). The intensity I_w of the secondary flow is represented by $w_{max} \sim \delta\varepsilon_1 az(F'_{10})_{max}$. The effect of the rheological properties on I_w can be characterized by the ratio $w_{max}/w_{new,max}$. Using the asymptotic expansions (28)–(31):

$$\frac{w_{max}}{w_{new,max}} \sim (1-r_0)\frac{\varphi_{new}}{\Pi^n \varphi^n_{new}}. \tag{76}$$

Comparatively to the Newtonian fluid, the intensity of the secondary flow is reduced because on one hand, the wall shear rate is higher, since ($\Pi > 1$) and on the other hand, the zone of shear flow is reduced by a factor of $(1-r_0)$. For low Hb, the above relation can be written as:

$$\frac{w_{max}}{w_{new,max}} \sim \varphi_{new}\left(\frac{n}{3n+1}\right)^n\left[1-\left(\frac{n}{2n+1}\right)\left(\frac{n}{3n+1}\right)^{n-1}Hb\right], \tag{77}$$

with

$$w_{new,max} \sim \varepsilon_1(az)\left(F'_{10}\right)_{new,max} \quad \text{and}$$
$$\left(F'_{10}\right)_{new,max} \approx 8.22\times 10^{-2}. \tag{78}$$

The upward flow near the heated wall (Fig. 2(b)) and the downward flow outside the thermal boundary layer induce a radial motion of the fluid particles. They enter the thermal boundary layer at the lower half of the duct, $0 < \phi < \pi/2$, and leave it at the upper half, $\pi/2 < \phi < \pi$. The asymptotic solution shows that:

$$v \sim -\frac{Gr}{Re}\left(\frac{az}{Pe}\right)^{4/3}\Psi_{10}\cos\phi. \tag{79}$$

The function Ψ_{10} represents the profile of v in the internal zone. As expected, v decreases with increasing r_0 (Fig. 6(c)). For $Pr \gg 1$, the relation (79) can be rewritten as

$$v \sim -\frac{Gr}{Re}\left[\frac{9X^+}{\varphi}\right]^{4/3}\frac{(1-r_0)}{\varphi^{n-1}}\Psi_{10,new}\cos\phi. \tag{80}$$

The axial flow is accelerated in the lower part of the duct as $(\delta\varepsilon_1 a^2 z)$ and decelerated with the same rate in the upper part. The modification of the axial velocity in

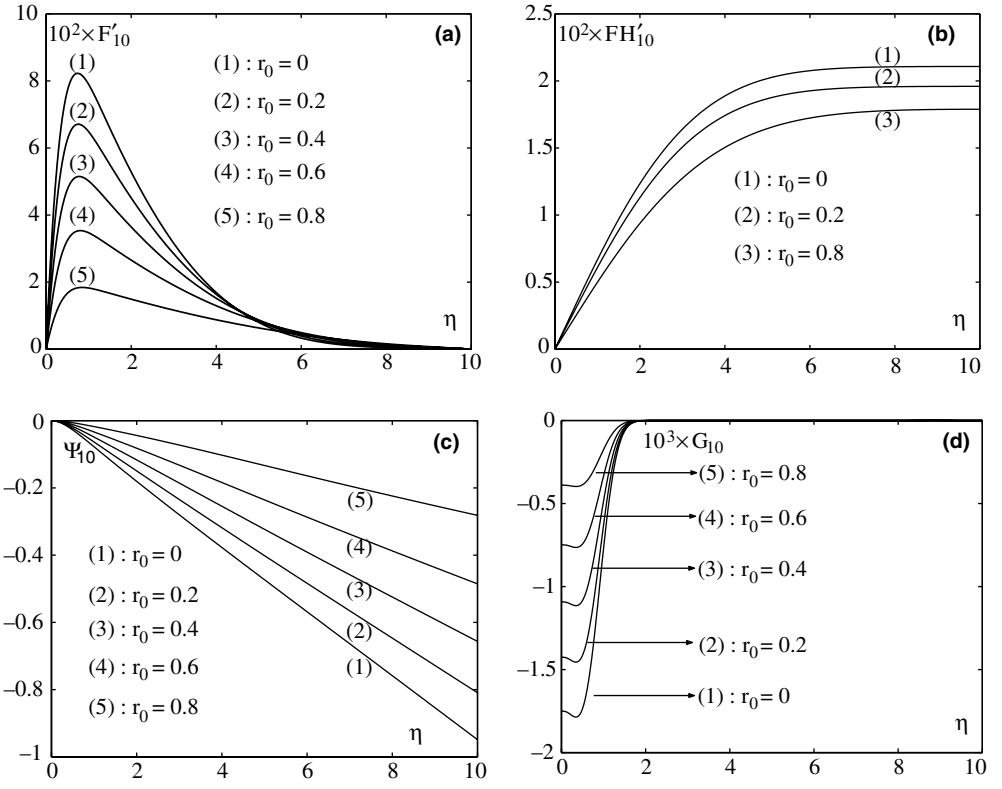

Fig. 6. Functions: (a) $F'_{10}(\eta)$; (b) $H'_{10}(\eta)$; (c) $\Psi_{10}(\eta)$ and (d) $G_{10}(\eta)$ for $n = 1$ and $Pr = 200$. (1) $r_0 = 0$; (2) $r_0 = 0.2$; (3) $r_0 = 0.4$; (4) $r_0 = 0.6$; (5) $r_0 = 0.8$.

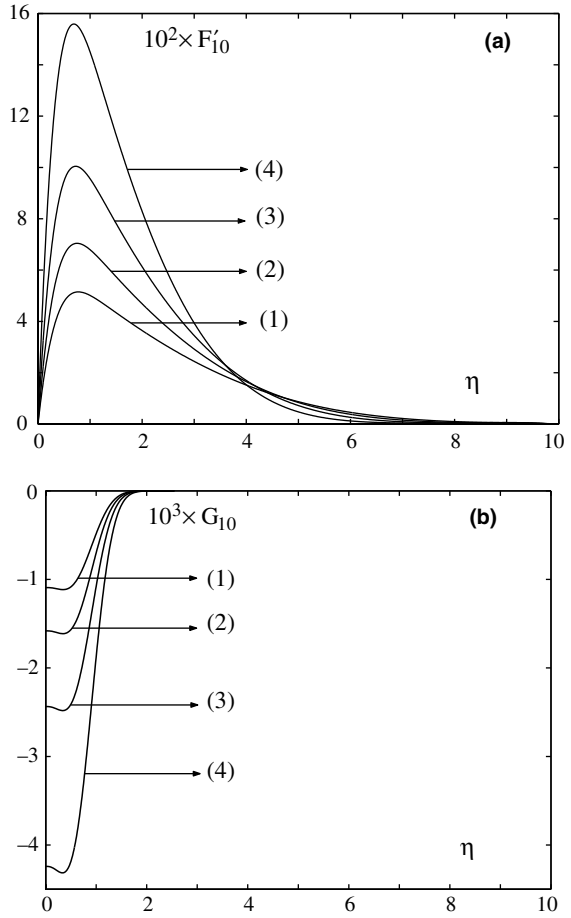

Fig. 7. Functions: (a) $F'_{10}(\eta)$ and (b) $G_{10}(\eta)$ for $Pr = 200$; $r_0 = 0.4$ and different flow behavior index, n. (1) $n = 1$; (2) $n = 0.8$; (3) $n = 0.6$; (4) $n = 0.4$.

the thermal boundary layer is represented by H'_{10}, shown in Fig. 6(b) for different r_0.

As far as the axial and azimuthal wall shear stresses are concerned, they are given by:

$$\tau^*_{rz} = \left[\frac{\tau^*_y}{2D^*_{II}} + K^*\left(2D^*_{II}\right)^{n-1}\right]\left(\frac{\partial u^*}{\partial r^*}\right);$$
$$\tau^*_{r\phi} = \left[\frac{\tau^*_y}{2D^*_{II}} + K^*(2D^*_{II})^{n-1}\right]\left(\frac{\partial w^*}{\partial r^*}\right). \quad (81)$$

Using the series expansion, it can be shown that the secondary flow effect on the wall shear stress can be described by:

$$\frac{\tau^*_{rz}}{\tau^*_{rz,fc}} \sim 1 + \varepsilon_1 (az)^{5/3}\frac{H''_{10}(0)\cos(\phi)}{\varphi}, \quad (82)$$

$$\tau^*_{r\phi} \sim \varepsilon_1 K^*_e \left(\frac{U^*_d}{R^*}\right)^n (az)^{2/3}\left[\frac{Hb}{\varphi} + \varphi^{n-1}\right]F''_{10}(0)\sin(\phi). \quad (83)$$

For $Pr \gg 1$, the above relation reduces to:

$$\frac{\tau^*_{r\phi}}{K^*_e (U^*_d/R^*)^n} \sim \frac{Gr}{Re}\left[\frac{9X^+}{\varphi}\right]^{2/3} F''_{10,new}(0)\sin(\phi), \quad (84)$$

with $F''_{10,new}(0) \approx 0.182$.

The upward flow of the warmer fluid near the heated wall and the downward flow of the cooler fluid outside the thermal boundary layer leads progressively to the appearance of a low density fluid layer with a higher temperature at the upper part of the duct. The colder fluid is confined in the lower part. The modification of the temperature profile is described by $G_{10}(\eta)$. The effect of r_0 and n on $G_{10}(\eta)$ are shown in Figs. 6(d) and 7(b). The temperature difference $[\theta]^t_b$ between the top and the bottom of the duct is:

$$[\theta]^t_b \sim 2\,Ra\,Pe^{1/3}\left[\frac{9X^+}{\Pi\varphi_{newt}}\right]^2 |G_{10}(0)|. \quad (85)$$

For a large Prandtl number, the numerical results presented in Fig. 6(d) and the asymptotic expansions indicate that the following approximation can be used: $|G_{10}(0)| \sim [(1-r_0)/\varphi^{n-1}]|G_{10}(0)_{new}|$, with $G_{10}(0)_{new} = -1.75\times10^{-3}$. This result can also be written in the form:

$$\frac{[\theta]^t_b}{[\theta]^t_{b,new}} \sim \frac{1-r_0}{\Pi^2\varphi^{n-1}}. \quad (86)$$

Once again, the effect of Hb on the temperature difference appears implicitly through the terms $(1-r_0)$ and Π.

The stratification of the thermal field induced by the upward flow of the warmer fluid induces an enhancement of the heat transfer in the bottom and a deterioration in the top. The asymptotic solution predicts the following relations:

$$\frac{Nu}{Nu_{fc}} \sim \frac{1}{1+\varepsilon_1(az)^{5/3}[G_{10}(0)/G_{00}(0)]\cos(\phi)}. \quad (87)$$

For $Pr \gg 1$

$$\frac{Nu}{Nu_{fc}} \sim 1 - Ra\frac{(1-r_0)}{\varphi^{n-1}}\left[\frac{9X^+}{\Pi\varphi_{new}}\right]^{5/3}\frac{G_{10,new}(0)}{G_{00}(0)}\cos(\phi), \quad (88)$$

where Ra is the Rayleigh number: $Ra = Gr \times Pr$.

Concerning the stresses within the pseudo-plug zone, similarly to the situation of forced convection with thermo-dependent consistency, it is shown that the stresses exceed the yield stress: $\tau^{pp}_{II} \sim (Hb/Re)^2 + \cdots$ In additions the (i,j)-components of the deviatoric stress tensor, $(i,j) \neq (r,z)$, or (z,r), tend to zero as the pseudo-yield surface is approached.

5.3. Mixed convection with thermo-dependent consistency $K^* = K(T^*)$

The decrease of K with increasing θ, on one hand reduces the drag forces of viscous origin, thereby

increasing the intensity of the secondary flow, and on the other hand increases the wall axial velocity gradient, which in turn decreases the thermal boundary layer thickness and therefore shifts the radial position of the maximum of the tangential velocity towards the wall. The modification of the tangential velocity profile by the thermo-dependency of K is shown in Fig. 8(a) for different r_0. The asymptotic solution indicates that:

$$w_{\max,\mathrm{th}} - w_{\max,n\mathrm{th}} \sim \frac{\varepsilon_1\varepsilon_2}{Pe^{1/3}}(az)^{4/3}F'_{11}(\eta_{\mathrm{wmax}}) \tag{89}$$

and

$$r(w_{\max,\mathrm{th}}) - r(w_{\max,n\mathrm{th}}) \sim \frac{\varepsilon_2}{Pe^{1/3}}(az)^{2/3}G_{01}(0). \tag{90}$$

The temperature difference $[\theta_{\mathrm{th}}]_{\mathrm{b}}^{\mathrm{t}}$ increases slightly as the numerical results of G_{11} in Fig. 8(d). As expected, with increasing r_0 or Hb, the temperature difference $[\theta_{\mathrm{th}}]_{\mathrm{b}}^{\mathrm{t}}$ reduces. The asymptotic solution gives

$$[\theta_{\mathrm{th}}]_{\mathrm{b}}^{\mathrm{t}} - [\theta_{n\mathrm{th}}]_{\mathrm{b}}^{\mathrm{h}} \sim -2\varepsilon_1\varepsilon_2(az)^{2/3}G_{11}(0). \tag{91}$$

Concerning the modification of the axial velocity, the combined effects of thermal stratification and the decrease of $K^*(T^*)$ tend to accelerate the fluid at the upper part of the duct as it is shown by the negative values of $H'_{11}(\eta)$ in Fig. 8(b). Finally the thermal stratification combined with the decrease of $K^*(T^*)$ tend to induce a radial motion of the fluid particles towards the wall at the upper part and to the core flow at the lower part of the duct (Fig. 8(c)).

6. Validity domain of the asymptotic solution

The asymptotic solution developed in this paper assumes that the forced convection is the dominant mechanism in the heat transfer and the natural convection is taken into account through a regular perturbation parameter. However, the intensity of the secondary flow induced by the buoyancy forces increases along the heating zone and the thermal stratification becomes more significant. From an axial position denoted X_{c}^{+}, the natural convection becomes the dominant convection mechanism and the asymptotic solution is no more valid. According to Bejan [28], the type of convection mechanism is decided by the smaller of the two scales of thermal boundary layer: $\delta_{\mathrm{t,fc}}$ (pure forced convection) and $\delta_{\mathrm{t,nc}}$ (pure natural convection).

In the situation of pure forced convection and a large Prandtl number, $Pr \gg 1$, using the energy equation, it can be shown that

$$\delta_{\mathrm{t,fc}} = \mathrm{O}\left[\left(\frac{X^{+}}{\Pi\varphi_{\mathrm{new}}\Pi'}\right)^{1/3}\right]. \tag{92}$$

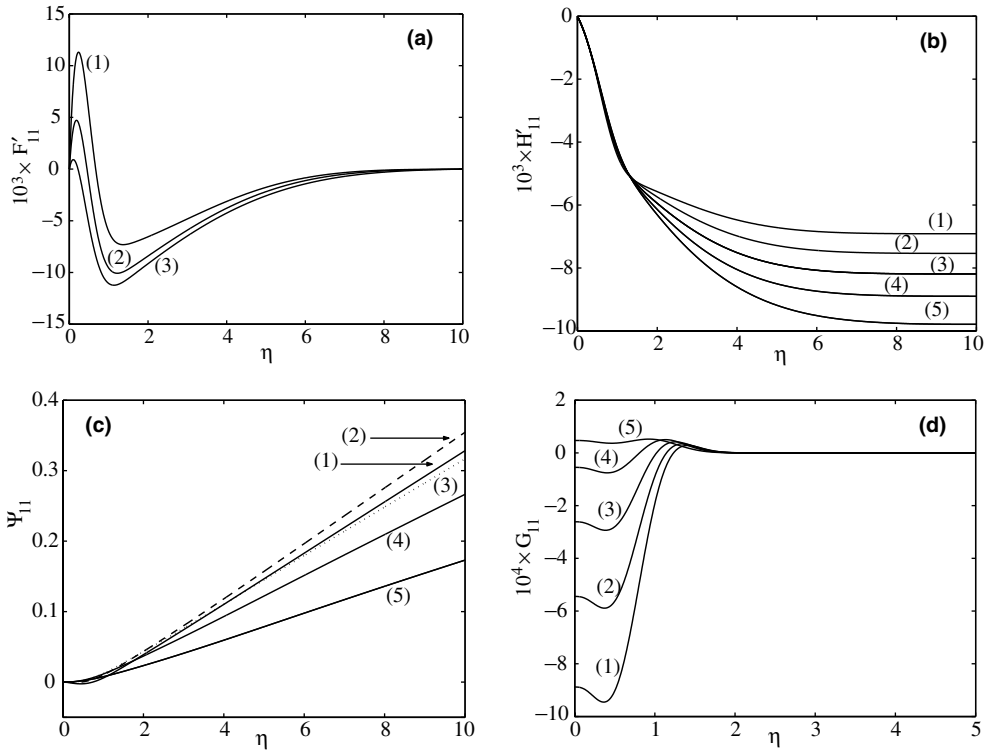

Fig. 8. Functions: (a) $F'_{11}(\eta)$; (b) $H'_{11}(\eta)$; (c) $\Psi_{11}(\eta)$ and (d) $G_{11}(\eta)$.

As it is indicated, the $K(\theta)$ variation affects the velocity distribution along the heating zone. However, in the thermal entrance region and for a large Prandtl number, the mechanical relaxation length is not significant, compared with the thermal relaxation length, that is the local velocity field adjusts almost instantaneously to the local temperature. Therefore, the temperature variation are small everywhere, except in a very thin thermal boundary layer. As a result, viscosity variations are not sufficiently large to cause significant variation in the pressure gradient. It then follows that the dependence of τ_{rz} upon z can be neglected [29,30]. This is consistent with Eq. (64), where it is shown that for large Pr, $\tau_{rz,\mathrm{th}}/\tau_{rz,\mathrm{nth}} = \mathrm{O}(\varepsilon_2^2)$. Hence, the decrease of the viscosity near the heated wall is offset by the increase of the wall shear rate. Then, the apparent viscosity μ_a^* can be approximated by: $\mu_a^* = \mu_0^*/\Pi'$, where $\mu_0^* = \mu_a^*(r = 1, z = 0)$.

For pure natural convection, the scaling analysis follows those performed for the boundary layer along infinite vertical plates [28]. When the Prandtl number is large, the thermal boundary layer $\delta_{\mathrm{t,nc}}$ is thin and is the location of the buoyancy force. Over $\delta_{\mathrm{t,nc}}$, combining on one hand a balance between thermal convection and thermal conduction (from energy equation) and on the other hand a balance between viscous and buoyancy forces (from momentum equation), we obtain

$$\delta_{\mathrm{t,nc}} = \mathrm{O}\left[\left(\frac{(\varphi_{\mathrm{new}})^{n-1}\Pi^{n-1}}{Ra\Pi'(1-r_0)}\right)^{1/5}\right]. \tag{93}$$

It is important to note that the same apparent viscosity is used for purely forced convection and for purely natural convection, since the same fluid has to be considered for the two convective mechanisms.

A new parameter E is defined by $E = \delta_{\mathrm{t,fc}}/\delta_{\mathrm{t,nc}}$:

$$E = \frac{\delta_{\mathrm{t,fc}}}{\delta_{\mathrm{t,nc}}} = \mathrm{O}\left[\frac{(X^+)^{1/3}Ra^{1/5}(1-r_0)^{1/5}}{(\Pi\varphi_{\mathrm{new}})^{n/5}(\Pi\varphi_{\mathrm{new}}\Pi')^{2/15}}\right]. \tag{94}$$

The transition from forced convection to natural convection dominant mechanism occurs approximately at $E = 1$. We define X_c^+, the critical Cameron number for which this condition is satisfied. When $E < 1$, $(X^+ < X_c^+)$, the forced convection dominates and when $E > 1$, $(X^+ > X_c^+)$, the natural convection dominates. It is clear that X_c^+ increases with increasing Hb.

To have an idea about the magnitude order of X_c^+, let us consider the electrical heat exchangers used in the thermal treatment of the fluid foods, the Rayleigh number is of order 10^4. This value is obtained using $\rho = 10^3$ kg/m^3, $\lambda = 0.6$ W/m °C, $\beta = 10^{-4}$ °C^{-1}, $K_e^* = 1$ Pa s^n, $n = 0.5$, $U_d^* = 0.2$ m/s, $R^* = 1.5 \times 10^{-2}$ m and $\Phi^* = 10^4$ W/m^2. Thus, X_c^+ is of order 10^{-2}. One can note that is much lower than the thermal entrance length, X_t^+, determined in the situation of forced convection: $X_t^+ = \mathrm{O}(1)$.

7. Conclusion

The characteristics of the thermal convection for a Herschel–Bulkley fluid flowing in a horizontal circular duct are investigated. As the Péclet number for the fluids considered in the present study is very large, an asymptotic analysis is then performed. The influence of the rheological parameters on the intensity of the secondary flows induced on one hand by the thermo-dependency of K^* and on the other hand by the buoyancy forces is determined. This influence arises from three different effects: (i) Variation of the wall shear rate, $\varphi = [Hb(1-r_0)/r_0]^{1/n}$, which control the thermal boundary layer thickness; (ii) variation of the shear thinning of the fluid; (iii) variation of the width of the yielded zone $(1-r_0)$. In order to understand how these individual effects contribute to the flow dynamics and heat transfer, three situations are considered: (i) forced convection with $K^* = K^*(T^*)$; (ii) mixed convection with $K^* = \mathrm{const.}$ and (iii) mixed convection with $K^* = K^*(T^*)$. Finally, useful relations are obtained for the heat transfer coefficient and the wall shear stress. The obtained results can be used for a Bingham or a power law fluid by setting $n = 1$ or $r_0 = 0$, respectively. In addition, similar expressions can be derived for an annular geometry or a plane channel, since the reasoning is based essentially on the assumption of a thin thermal boundary layer.

Acknowledgements

The author is grateful to Dr. M. Mamou and Pr. J.P. Brancher for fruitful discussions. The referees are thanked for their constructive comments.

References

[1] Y.I. Cho, J.P. Hartnett, Non-Newtonian fluids un circular pipe flow, Advances in Heat Transfer, vol. 15, Academic Press, New York, 1982, pp. 59–141.
[2] A.V. Shenoy, R.A. Mashelkar, Thermal convection in non-Newtonian fluids, Advances in Heat Transfer, vol. 15, Academic Press, New York, 1982, pp. 143–225.
[3] R. Bird, G.C. Dai, B.J. Yarusso, The rheology and flow of viscoplastic materials, Rev. Chem. Eng. 1 (1983) 1–110.
[4] E. Hirai, Theoretical explanation of heat transfer in the laminar region of a Bingham fluid, A.I.Ch.E. J. 5 (1959) 130–133.
[5] E.H. Wissler, R.S. Schechter, The Graetz–Nusselt problem (with extension) for a Bingham plastic, Chem. Eng. Progr. Symp. Ser. 29 55 (1959) 203–208.

[6] B.F. Blackwell, Numerical solution of the Graetz problem for a Bingham plastic in laminar tube flow with constant wall temperature, ASME J. Heat Transfer 107 (5) (1985) 466–468.
[7] P.R. Johnston, Axial conduction and the Gratez problem for a Bingham plastic in laminar tube flow, Int. J. Heat Mass Transfer 34 (1991) 1209–1217.
[8] T. Min, J.Y. Yoo, H. Choi, Laminar convective heat transfer of a Bingham plastic in a circular pipe. I. Analytical approach-thermally fully developed flow and thermally developing flow (the Graetz problem extended), Int. J. Heat Mass Transfer 40 (13) (1997) 3025–3037.
[9] T. Min, J.Y. Yoo, Laminar convective heat transfer of a Bingham plastic in a circular pipe with uniform wall heat flux: the Graetz problem extended, ASME J. Heat Transfer 121 (8) (1999) 556–563.
[10] G.C. Vradis, J. Dougher, S. Kumar, Entrance pipe flow and heat transfer for a Bingham plastic, Int. J. Heat Mass Transfer 36 (3) (1993) 543–552.
[11] T. Min, H.G. Choi, J.Y. Yoo, Laminar convective heat transfer of a Bingham plastic in a circular pipe. II. Numerical approach-hydrodynamically developing flow and simultaneously developing flow, Int. J. Heat Mass Transfer 40 (15) (1997) 3689–3701.
[12] G. Forrest, W.L. Wilkinson, Laminar heat transfer to temperature-dependent Bingham fluids in tubes, Int. J. Heat Mass Transfer 16 (1973) 2377–2391.
[13] M. Naïmi, R. Devienne, M. Lebouché, Etude dynamique et thermique de l'écoulement de Couette–Taylor–Poiseuille: Cas d'un liquide présentant un seuil d'écoulement, Int. J. Heat Mass Transfer 33 (1990) 383–391.
[14] C. Nouar, R. Devienne, M. Lebouché, Convection thermique dans la région d'entrée d'une conduite, Int. J. Heat Mass Transfer 37 (1994) 1–12.
[15] C. Nouar, C. Desaubry, H. Zenaïdi, Numerical and experimental investigation of thermal convection for a thermo-dependent Herschel–Bulkley fluid in an annular duct with rotating inner cylinder, Eur. J. Mech. B/Fluids 17 (1998) 875–900.
[16] M. Soares, M.F. Naccache, P.R. Souza Mendes, Heat transfer to viscoplastic materials flowing laminarly in the entrance region of tubes, Int. J. Heat Fluid Flow 20 (1999) 60–67.
[17] N. Patel, D.B. Ingham, Analytic solutions for the mixed convection flow of non-Newtonian fluids in parallel plate ducts, Int. Commun. Heat Mass Transfer 21 (1) (1994) 75–84.
[18] N. Patel, D.B. Ingham, Mixed convection flow of a Bingham plastic in an eccentric annulus, Int. J. Heat Fluid Flow 15 (2) (1994) 132–141.
[19] G. Deschamps, O. Terral, P. Terrien, Tube à passage de courant. Echangeur électrique, Technique de l'Ingénieur, Traité Génie Energétique, BE 9 542 (2000) 1–18.
[20] C. Nouar, B. Benaouda, C. Desaubry, Laminar mixed convection in a horizontal annular duct. Case of thermo-dependent non-Newtonian fluid, Eur. J. Mech. B/Fluids 19 (2000) 423–452.
[21] M. Van Dyke, Perturbation Methods in Fluid Mechanics, Academic Press, New York, 1964, pp. 85–88.
[22] A.W. Bush, Perturbation Methods for Engineers and Scientists, CRC Press, 1992, p. 13 (Chapter 1) and p. 177 (Chapter 5).
[23] G.I. Barenblatt, Scaling, Self Similarity, and Intermediate Asymptotics, Cambridge Texts in Applied Mathematics, Cambridge University Press, 1996, pp. 161–180 (Chapter 6).
[24] M.A. Lévêque, Les lois de transmission de la chaleur par convection, Ann. Mines 37 (1928) 201–299, 305–362, 381–415.
[25] I.C. Walton, S.H. Bittleston, The axial flow of a Bingham plastic in a narrow eccentric annulus, J. Fluid Mech. 222 (1991) 39–60.
[26] N.J. Balmorth, R.V. Craster, A consistent thin-layer theory for Bingham plastics, J. Non-Newtonian Fluid Mech. 84 (1999) 65–81.
[27] I.A. Frigaard, D.P. Ryan, Flow of a visco-plastic fluid in a channel of a slowly varying width, J. Non-Newtonian Fluid Mech. 123 (1) (2004) 67–83.
[28] A. Bejan, Convection Heat Transfer, second ed., John Wiley, New York, 1994, pp. 188–191.
[29] H. Ockendon, J.R. Ockendon, Variable viscosity flows in heated and cooled channels, J. Fluid Mech. 83 (1977) 177–190.
[30] S.M. Richardson, Flow of variable viscosity fluids in ducts with heated walls, J. Non-Newtonian Fluid Mech. 25 (1986) 137–156.